3D printed mould-based Graphite/PDMS sensor for low-force applications

A. Nag[1,*], S. Feng[1], S. C. Mukhopadhyay[1], J. Kosel[2] and D. Inglis[1]

[1]School of Engineering
Faculty of Science and Engineering
Macquarie University
Sydney, NSW 2109, Australia
[2]Computer, Electrical, Mathematical, Science and Engineering Division
King Abdullah University of Science and Technology (KAUST)
Saudi Arabia
*Corresponding author email: anindya1991@gmail.com
The contributions of the first and second authors are the same.

Abstract— **This paper concerns the design, fabrication and characterization of graphite/PDMS sensors for low-force sensing applications. Exploiting the design flexibility of 3D printing, moulds of specific dimensions were prepared onto which graphite powder and PDMS were cast, to develop sensor patches. The sensor patches were highly flexible with repeatable responses to iterative bending cycles. The patches were tested in terms of stretchability, strain and bending-cycle responses. The sensor patches had interdigitated electrodes operating on capacitive sensing, where the effective capacitance changes with an applied force because of changes in their dimensions. Forces ranging from 3.5 mN to 17.5 mN were applied to determine the capability of these sensor patches for low-force sensing applications. The sensor patches had a quick recovery having a sensitivity and SNR per unit force of 0.2542pF.mN^{-1} and 10.86 respectively. The patches were capable of differentiating the forces applied on them, when they were attached to different objects in daily use.**

Keywords—Graphite; PDMS; 3D printing; Force sensing; Capacitive sensor.

1. Introduction

The use of force sensors is a popular and convenient technique in sensing technology for monitoring different strain-induced applications. They have always been a popular choice due to their benefits for dynamic and quasi-static measurements. Different kinds of force sensors based on the processed materials, operating principle, and performance have been developed to date. The advantages of these force sensors lie in the longevity in their performances in terms of sensitivity, linear range of operation and durability with various loads. In earlier times, force sensors with silicon-based substrates were developed for industrial [1, 2] and biomedical [3, 4] applications. Even though they did serve a wide range of interdisciplinary applications like imaging and interventional fields [5], there were certain disadvantages attached to them. Some of them are high cost per unit, low output signal, high input power and high leakage current. As a result of these drawbacks, sensors with flexible materials [6] have been devised and formulated for force sensing [7, 8]. In order to develop flexible sensor prototypes, a range of processing material have been used based on their electrical, mechanical and thermal properties. Different types of polymeric and elastomeric materials like polydimethylsiloxane (PDMS) [9], polyethylene terephthalate (PET) [10], polyimide (PI) [11], poly(3,4-ethylenedioxythiophene) polystyrene sulfonate (PEDOT:PSS) [12], etc. have been used to develop the substrate of the flexible force sensors. Among these materials, PDMS has been a favourite choice [13-15] due to the low cost, hydrophobicity, biocompatible nature, easy handling in combination with a moulding process and ability to form nanocomposites due to the formation of exceptional interfacial covalent bonding with the electrodes [16]. Similarly, different types of conductive materials like carbon allotropes [17], silver [18], gold [19] have been used to develop the electrodes of the sensor patches. The choice of conductive material differs in terms of their electro-mechanical properties. Graphite, one of the allotropes of carbon, has been used predominantly due to its high electrical conductivity, porosity, and corrosion resistance compared to other allotropes of carbon as electrodes. They have been used for temperature sensing [20, 21], electrochemical sensing [22, 23], strain sensing [24], piezo-resistive sensing [17] and bio-sensing [25-28]. Among the fabrication techniques, different methodologies like photolithography [29], screen printing [30], laser cutting [31], 3D printing [32], etc. have been used for developing flexible prototypes. Among them, utilizing 3D printing to develop the moulds [33, 34] provides a high degree of design flexibility, which could be exploited to optimize the sensor design for specific applications. This paper presents the design, development, and implementation of novel sensor patches fabricated by combining 3D printing with a casting technique. 3D printing was used to produce a

mould for the desired sensor shape into which a thin layer of graphite powder was filled followed by casting in PDMS. This process results in flexible sensor patches with conductive graphite electrodes at their top surface. After curing, the developed sensor was peeled out of the mould, characterized and used for force sensing.
Nowadays, flexible sensors incorporated with microelectromechanical systems (MEMS) have become a popular choice for researchers to develop micro-structured devices for force sensing. Some of the applications include their uses as tactile sensors for biomimetic application [35] and robotic applications [36], while some of the sensors, being capacitive in nature, offering the advantages of simplicity in design and fabrication, high sensitivity, and relatively low energy consumption [37]. The application of flexible sensors for [38] applied low-force sensing specially in the field of tactile sensing, [39] used it for robotic and upper-limb prostheses, touch screens were made using it by [40] and soft tactile sensors were achieved using it by [41]. Although various materials have been used in this research, there have been certain limitations like high cost, complexity in design and rigidity associated with them. For example, even though [38] used a microfluidic multilayer sensor to measure forces up to 2.5 N, their disadvantages lie in the material cost and complexity of the structure. Although, the research from [42] on capacitive polymer tactile sensors is available, the detectable range of operation in this case is too high, especially for haptic robotic applications. Our work provides a conjunctive approach on the cost of fabrication, operating principle and detectable range. Our sensors can also detect forces within a low-force regime, ranging from 3.5 mN to 17.5 mN, which could lead to utilization of these sensors as wearables for rehabilitation purposes after the patient suffers from a stroke, muscle spasms, etc. In such cases the sensors would enable monitoring of even slight movements of a body part to determine the patient's recovery. The novelties of this paper lie in two specifics: (i) the development of a flexible, capacitive sensor patch fabricated using a 3D printed mould and (ii) the application of these sensor patches for low-force sensing.

2. Fabrication of the sensor patches

The fabrication of the sensor patches was done in the laboratory environment at fixed temperature and humidity conditions. Figure 1 shows a schematic of the steps carried out for fabrication of the sensor patches. A 3D printer (3D PRINTING SYSTEMS, UP Plus 2) was used for creating the moulds, which were employed as reusable templates to fabricate the sensor patches. [43] showed the use of Acrylonitrile Butadiene Styrene (ABS), with a diameter of 1.75 mm being the best 3D printer filament. A printed-circuit board acted as the base onto which the mould was printed (Figure 1(A)). The design of the electrodes was done with commercial software (CREO Parametric 2.0) that related to the printing system. The fabrication of a 3D printed mould (Figure 1(B)) took around 25 minutes. The moulds were thoroughly cleaned with isopropanol before using them for casting purposes. The initial casting was done with graphite powder (Sigma-Aldrich 282863-25G, <20 µm) onto the trenches of the 3D printed moulds (Figure 1(C)).

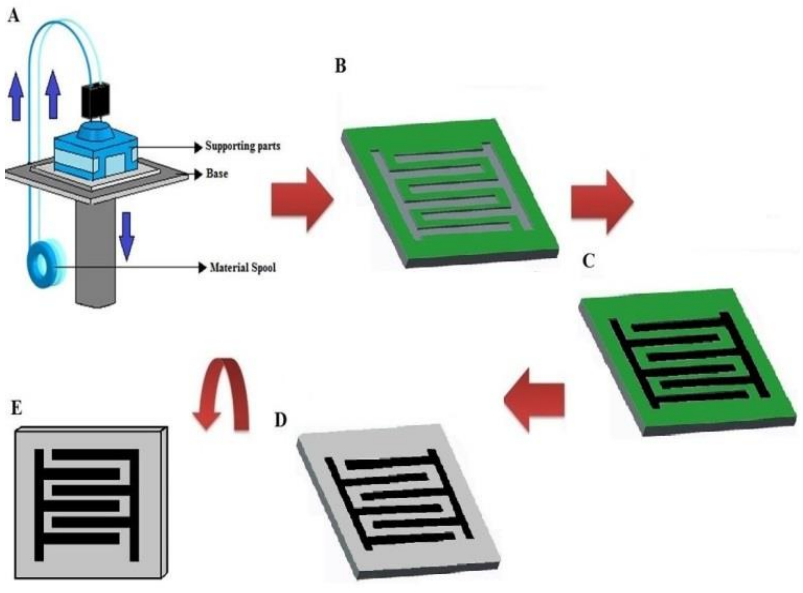

Figure 1: Schematic diagram of the fabrication process. (A) 3D printing resulted in the reusable mould (B). Then, graphite powder was cast (C) onto the mould, filling its trenches. This was followed by casting of PDMS (D), which was cured to form the sensor patches (E).

The residual powder remaining on the moulds other than on the trenches was carefully scraped off. Then, a layer of PDMS (SYLGARD® 184 SILICONE ELASTOMER KIT) was cast onto the mould to form the substrate of the sensor patches (Figure 1(D)). The height of the PDMS layer was adjusted to 1000 microns by a casting knife (SHEEN, 1117/1000mm) (Figure 1(D)). The sample was then desiccated for an hour to remove any trapped air bubbles on the surface of the PDMS (Figure 1(D)). After curing of the sample in the oven at 70 °C for 2 hours, it was peeled off to generate the final sensor patch (Figure 1(E)). A study was performed to determine the concentration of graphite used in the trenches of the mould to develop the electrodes. A trade-off was done between the electrical conductivity and the mechanical flexibility of the resultant electrodes to determine the amount of graphite powder.

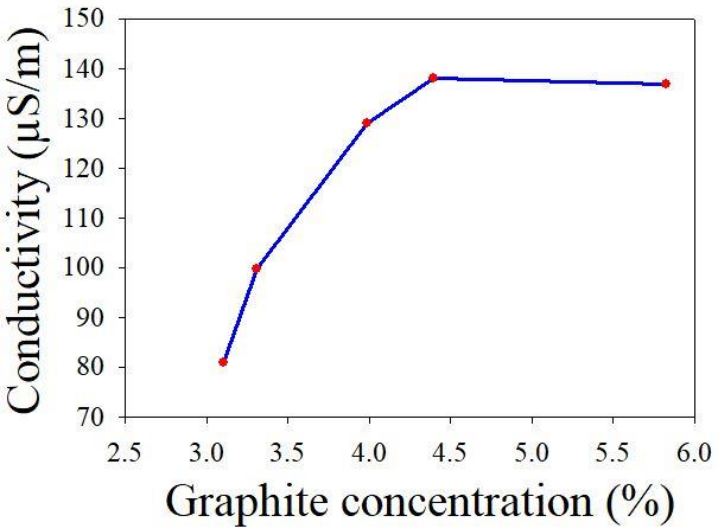

Figure 2: Change in conductivity as a function of the graphite powder.

The result in Figure 2 shows the change in conductivity with the concentration of graphite present in the total mass of graphite and PDMS. It is seen that the conductivity of the electrodes gradually increases with an increasing concentration of graphite in the mixture until 4.4 %, after which it remained almost constant. The amount of graphite powder and PDMS on the electrodes varied in accordance with the height of the trenches, thus keeping the ratio constant. This happened due to the percolation threshold of the nanofillers in PDMS, causing a saturation of the interfacial bonding between the conductive materials. The gradual increase in the amount of graphite powder increased the linkage of the nanofillers, thus increasing the electrical conductivity constructing an interconnected network in the polymer matrix. Even though the resultant electrical conductivity of the nanocomposite-formed electrodes were less than that of graphite, the overall conductivity was good enough for this force-sensing application.

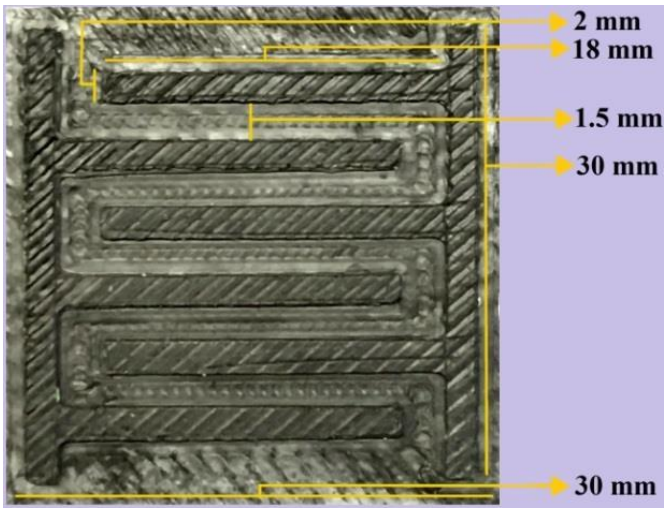

Figure 3: Front view of the final sensor patch. The sensor patch consisted of three pairs of electrode fingers, each with a length and width of 18 mm and 2 mm, respectively. The interdigital distance was 1.5 mm and the sensor patch had a total surface area of 900 mm^2.

Figure 3 shows a front view of the sensor patch obtained at the end of the fabrication process. The sensor patch, having a surface area of 900 mm^2, consisted of three pairs of electrode fingers, each having a length (L) and width (W) of 18 mm and 2 mm, respectively. The interdigital distance (d) between two consecutive fingers was 1.5 mm. The thickness of the sensor patches was around 2 mm. Figure 4 shows the top view and cross-sectional view of Scanning Electron Microscope (SEM) images of the developed sensor patch taken with a Phenom XL. The PDMS layer came off smoothly and cleanly from the top of the graphite electrodes (Figure 4(A)). A top view of the electrodes, representing the graphite and PDMS mixture with black and white regions respectively, is shown in Figure 4(B). The image was taken near the centre of one of the electrode fingers which justifies the presence of a higher amount of graphite than of PDMS. The cross-sectional view of the electrodes is shown in Figure 4(C), which shows the two distinct layers of PDMS substrate and graphite and PDMS mixed electrodes. It is seen that the edges of the electrodes came off clean and perpendicular to the surface, formed by the curing process of PDMS and peeling the sensors off the 3D-printed moulds. A comparison between the size of the final product and a 50 cent AUD is shown in Figure 5.

An illustration of the flexibility of the sensor patches is shown in Figure 6. The significance of this high mechanical deformation of the sensors lies in their usages for precise strain-induced applications like in aircrafts, military applications, tissue engineering, environment, energy harvesting, etc. The capability of these sensors to immediately reform to the original state without the occurrence of any offset value (Figure 12) makes a viable option to be used for a long term with getting replaced. The consistency of the results (shown below) makes them popular for smart-home related applications where the usage of seating objects like chair, couch, etc. can be monitored and determined accurately. The characterization and experimental tests of the sensor patches were carried out using an impedance analyser (HIOKI IM 3536 High tester). Kelvin probes were used to connect the patches from one end while they were attached to clamps or bent during the characterization procedure. For the experiments, the sensor patches were firmly fixed at the opposite end of the Kelvin probe to determine the changes because of the applied load.

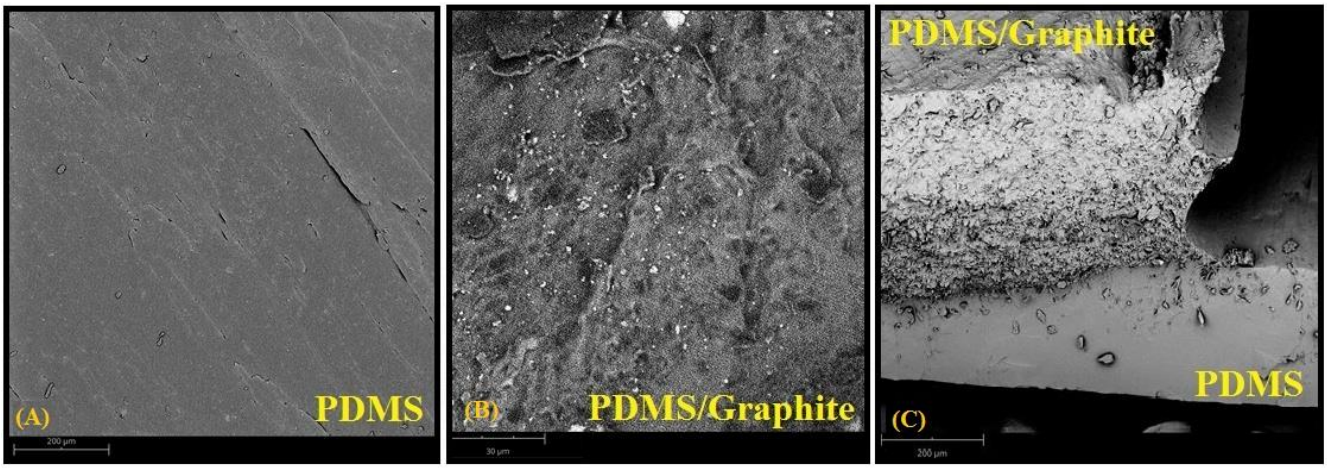

Figure 4: SEM images of the developed graphite-PDMS sensor depicting the top-view of (A) PDMS, (B) graphite-PDMS mixture and (C) cross-sectional view of the electrodes.

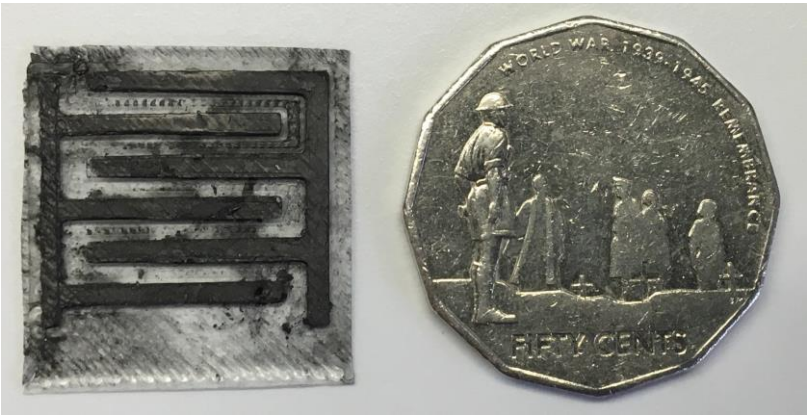

Figure 5: Comparison of the size of the sensor patch with a 50 cent AUD.

Figure 6: Image of the developed sensor patch depicting its flexibility.

3. Operating Principle

The working principle of the sensors can be compared with that of a planar capacitor. Due to the flexible nature of the patches, their dimensions changed as a result of an external load on their sensing area. [44] roughly defined the relative change in capacitance of a flexible sensor as

$$\frac{\Delta C}{C} = \left(\frac{\Delta A}{A} - \frac{\Delta d}{d}\right) \quad \text{(i)}$$

where, $\frac{\Delta C}{C}$ is the relative capacitance, $\frac{\Delta A}{A}$ and $\frac{\Delta d}{d}$ are the relative changes in area and interdigital distance respectively.

The total area (A) can be related to the length (L) and width (W) of the electrodes. So, eq. (i) can be rewritten as,

$$\frac{\Delta C}{C} = \left(\frac{\Delta L}{L} + \frac{\Delta W}{W} - \frac{\Delta d}{d}\right) \quad \text{(ii)}$$

On the application of an external force F, the effective Young's Modulus (Y) of the sensor changes, along with its dimensions (length (L + ΔL), width (W + ΔW) and interdigital distance (d + Δd) of the electrodes) [45, 46]. Thus, the relative change in capacitance with respect to load can be given by eq. (iii),

$$\frac{\Delta C}{C} = \frac{2F}{AY'} \quad \text{(iii)}$$

where, F is the external force applied and Y' is the effective Young's modulus.

The equivalent model of the developed sensor was determined using a theoretical model performed by a spectrum-analyser algorithm. The non-linear least-square curve-fitting (CNLS) technique was applied on the sensor to determine its electrical parameters. This was achieved by obtaining the profile of the sensor in air without any given load. Figure 7 shows the Nyquist plot (red dotted line) obtained from a frequency sweep done between 1 Hz and 100 kHz, being fitted to the theoretical estimated values (green line) to obtain the suggested circuit. The equivalent circuit shown in the inset of Figure 7 shows the presence of the two capacitive elements and one resistive element of the sensor. In addition to the capacitive nature (C1) of the interdigitated electrodes and resistance (R) of the material, the second capacitive element (C2) is due to the double-layered capacitance created by the connection of the sensor with the probes.

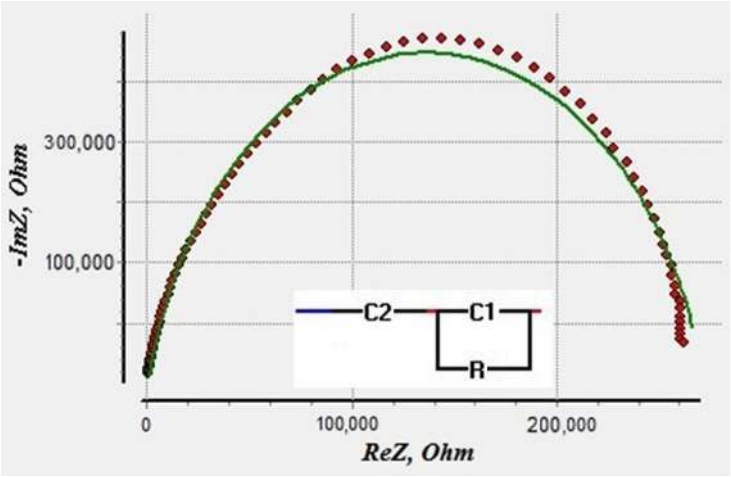

Figure 7: Equivalent circuit of the sensor determined through profiling of the sensor done in air.

4. Experimental results

The characterization of the sensor patches was carried out at 5 kHz. Initially, a load-extension measurement was done with the sensor patches to determine their elastic behaviour. The experiments were performed with a 10 kN tensile tester (EXCEED Model E42) as shown in Figure 8. The sensor patch was clamped from two sides with the electrode fingers parallel to the clamped regions. The direction of the applied load is shown in the inset of Figure 8. The load was applied on the sensor patch by fixing one of the two clamps while moving the other one. As shown in Figure 9, the response is within the elastic limit of the load-extension curve and the extension follows linearly the applied load with a high regression coefficient. It is seen that the yield point, ultimate stress and rupture point of the sensors are 13.9 N, 14.41 N and 14.13 N respectively. The Young's Modulus (E) of the sensor patches at an extension of 6 mm was 163.6 kPa, obtained from the calculated values of stress (81.8 kPa) and strain (0.5).

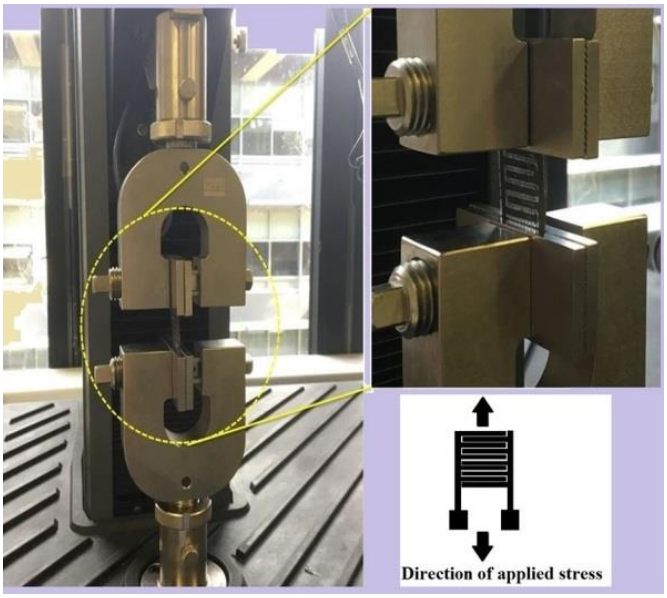

Figure 8: Experimental setup for load-extension measurements. The inset shows the direction of the applied load.

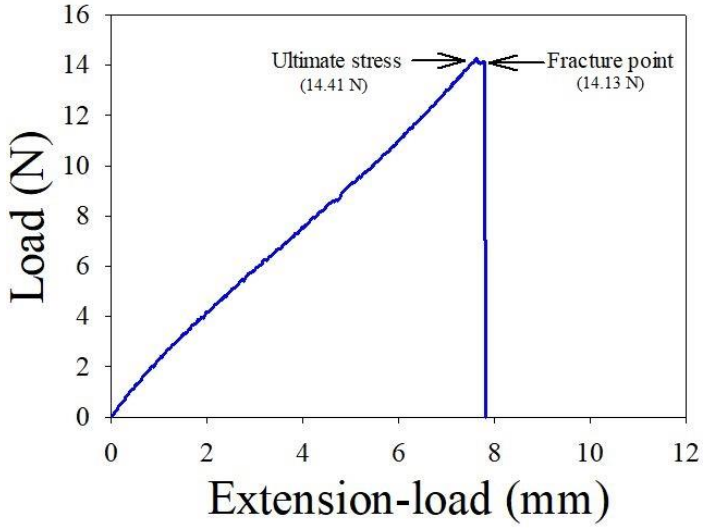

Figure 9: Response of the sensor in terms of extension with respect to an applied load.

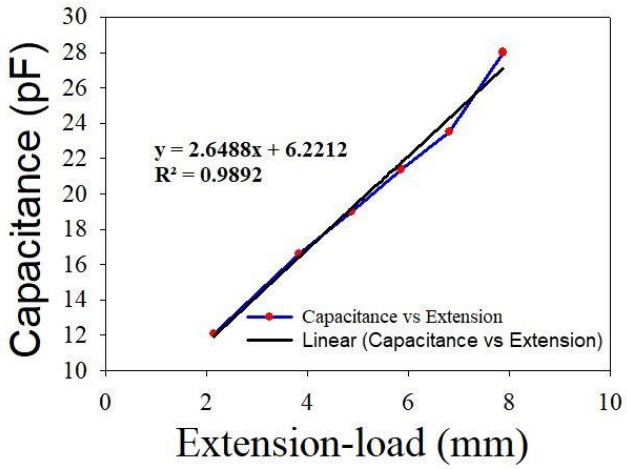

Figure 10: The capacitance of the sensor patch when extended by an applied load.

The change in capacitance of the patch because of the extension is shown in Figure 10. It was almost linear, with a sensitivity of

$$\text{Sensitivity} = \Delta C / \Delta \text{Extension} = 2.5 \text{ pF/mm} \qquad \text{(iii)}$$

The bending response of the sensor patches was tested by bending them by hand so that the electrodes were under compressive load. Figure 11 shows the different capacitance values for bending radii of curvature ranging from 6 mm to 11 mm. A controlled bending was done by applying a constant force on the sensing area using a force gauge, while fixing the two sides of the sensor between the marked table tops. The marking was done (in mm range) to determine the changes of the radius of curvature of the sensor. The applied force was changed simultaneously vary the bending radius, followed by obtaining the capacitance value at a particular radius. The capacitance decreased with increasing radius. As the condition of the sensor patch changed between the normal and flexed state, the dimensions of the sensor patch oscillated between the normal and compressed. Having an insight of the increase and decrease in capacitance for the tensile (extension) and compressive (bending) stresses respectively, there would an overall increase in the capacitance when both stresses affect the sensor simultaneously [46, 47]. One common example for this type of application is the detection of body movements, where the sensors attached to the joints of the limbs would experience an overall strain as a result of their flexed condition. The overall increase in the capacitance can be attributed to a higher effect of the applied stress on the area (A) than on the interdigital distance (d) of the electrodes. Figure 12 shows the change in the capacitance for the normal and bent states of the sensor patch undergoing 10 cycles. The bending was done manually by hand, as shown in the inset ((a) and (b)) of Figure 12. The consistency of the bending radius of the sensor was ensured by bending the

sensor to the smallest possible curvature (3 mm). When the sensor patch changed from normal to a bent state, the capacitance value increased from 2 pF to an average value of 35 pF. The switching action of the capacitance values can be attributed to the change in dimension of the sensor. This happens due to a decrease in the radius of curvature due to the bending of the patch, which increases the capacitance value, as is evident from Figure 11. However, there were minor glitches (1st and 8th cycles) in capacitance values, which can be attributed to human error. Overall, the sensors did display consistent results for this specific bending radius.

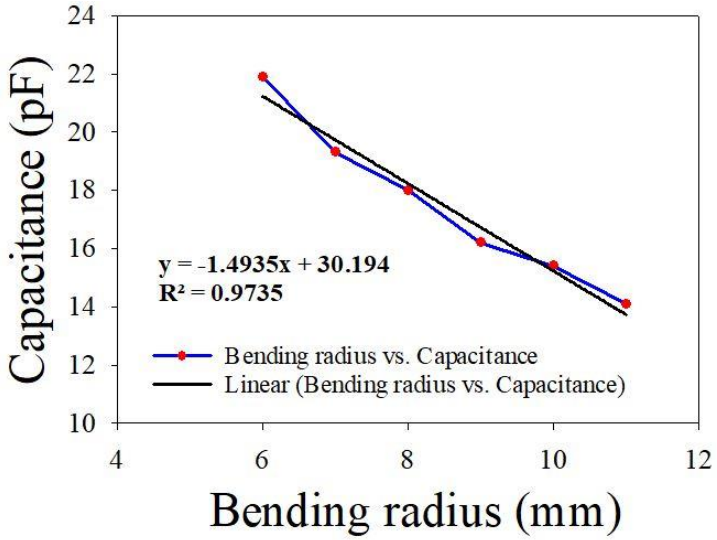

Figure 11: Capacitance of the sensor for a bending radius from 11 mm to 6 mm.

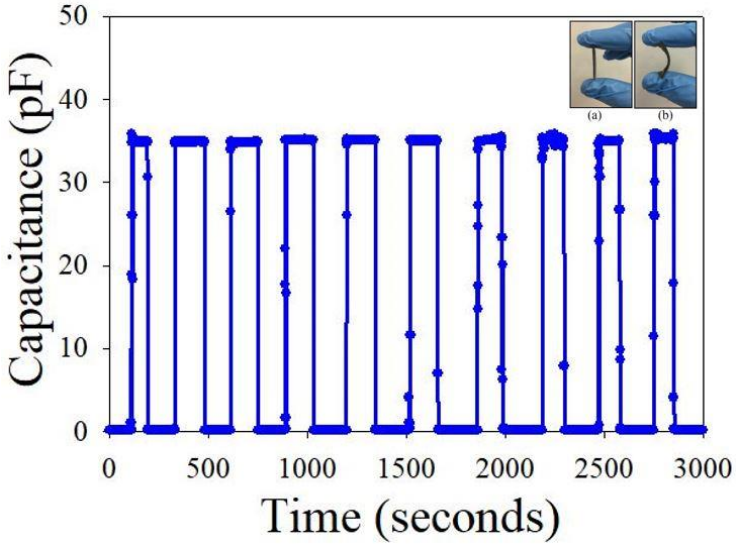

Figure 12: Capacitance of the sensor patch for multiple cycles of normal and bent states. The capacitance value increases in the bending state compared to the normal state of the patch.

Force-sensing experiments were conducted with different weights of the same shape by placing them on the sensor patches. The sensor patches were tested with five different forces, ranging from 3.5 mN to 17.5 mN. The patches were firmly fixed to avoid any movements during experimentation. The location of the weights on the sensing area of the patches were kept the same to minimize the effects of their area on the responses. An average of five experimental readings was taken for each weight to ensure repeatability of their responses. A particular frequency (5 kHz) was chosen to determine the different capacitance values with respect to the forces. Figure 13 shows the response of the sensor patches for the five loading forces. As shown in the figure, the change in capacitance values with respect to the forces is almost linear, with a force sensitivity of $0.2542 pF.mN^{-1}$, in a range from 3.5 mN to 17.5 mN.

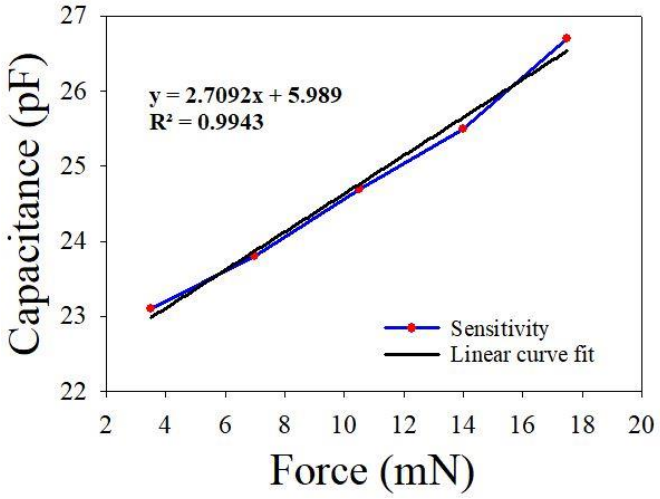

Figure 13: Response of the sensor patch for a particular frequency (5 kHz) depicting the different capacitance values for the different experimental weights.

Some possible real-time applications with the developed sensor patches are shown in Figure 14. Biocompatible tapes (STAPLES masking tape) were used to attach the sensor patches to different objects like a ball (20.04 gm), a cup (320.85 gm), a bottle (379.18 gm) and a badminton (98 gm) racket. The responses of the sensor patches were determined to analyse the force with which the objects were held. Figure 15 gives the different capacitance values with respect to each object. The forces were applied with the hand on the sensing area of the patches. It is seen from the values that the sensor patches were capable of differentiating the forces exerted on each object. This is advantageous in two ways,

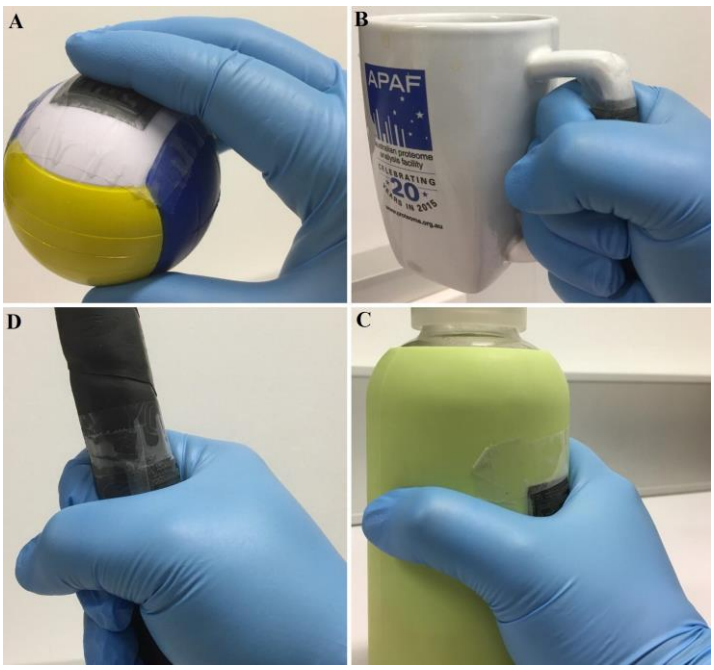

Figure 14: Illustration of some possible applications in force sensing with the fabricated sensor patches. The patches were attached on the (A) Ball (B) Cup (C) Bottle and (D) Racket to test their usages.

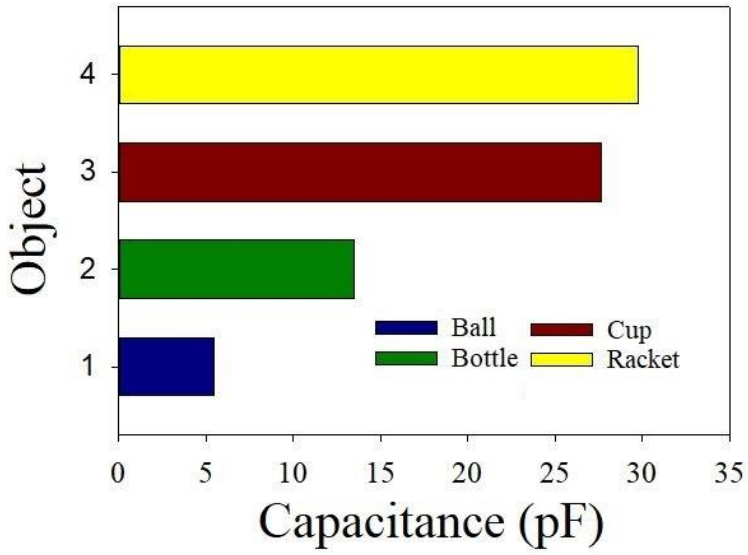

Figure 15: Response of the sensor patches for the above applications. The differences in the responses were present due to the different forces worked on the sensor patch.

Firstly, these Graphite/PDMS patches can also be attached to other daily-use objects to test their usages. Also, they have an advantage for tactile sensing with various prosthetic limbs, where the amount of force exerted on the sensors can be analysed with these artificial limbs. Apart from the simple operating principle and large-scale fabrication of these sensor patches at low cost, other advantages of these patches lie in their robustness in terms of mechanical flexibility and capability of sensing very low forces which makes them a popular choice for real-time force sensing applications.

5. Conclusion

This paper presents the development and implementation of some novel flexible force sensors, which were fabricated using 3D printed moulds. The sensor patches were fabricated by casting of graphite and PDMS into these moulds. Graphite, being one of the most conductive allotropes of carbon, was used due to its high electrical conductivity and corrosion resistance. PDMS was used to develop the substrates due to its low-cost and easy handling. The curing of the PDMS layer formed the sensor patches, which were then characterized and used for low force sensing applications. This method combines the flexibility of 3D printing in terms of geometries with a cost-effective casting process. Interdigitated electrodes on top of the patches were used for sensing the effects of forces applied to the patches by measuring the capacitance of these structures. The sensor patches were characterized with respect to load, extension and bending. Table 1 shows a comparative study of some of the important parameters like fabrication techniques, materials used, sensitivity, limit of detection and range for some of the significant research work done on force and pressure sensors. In comparison to all this work, the novelty of our work lies in the conjugated use of 3D printing and casting techniques to develop flexible force sensors. The moulds can be reused many times, and large-scale production of these sensors makes it a quick and efficient fabrication process. The thin-film nature of these sensors makes them viable to be used for multifunctional strain-induced applications. The inclusion of Graphite and PDMS, both of which are cheap and biocompatible, for force sensing creates an alternative to the expensive force-sensing systems used in industry. In terms of fabrication procedure, the Graphite content in PDMS used to develop the nanocomposite-formed electrodes can also be utilized to form multilayered thin-film structures. The capacitive nature of these sensors adds to the overall low cost of operation in terms of low input power. Another major advantage is the stability of the response, as shown from consecutive bending cycles. It can be very significant for the 3D printed devices whose responses saturate after prolonged use. This can be an expensive process if replacement of sensors is needed to maintain constant sensitivity. Even though the results for just ten cycles have been shown in the manuscript, the response did not change after continuous bending of more than hundred cycles. The stability of this response can be attributed to two factors. The formation of the nanocomposite-based electrodes included the synergic effects of graphite and PDMS, adding robustness and flexibility to them [48]. The interconnected nanocomposite sensing network allowed free movement of the nanofillers, thus negating any brittle nature of the electrodes. Secondly, due to the high aspect ratio of graphite nanoparticles [49, 50], there would be an improvement in contacts between the nanoparticles subsequent to mechanical deformation. This allows the structure to get back into its original position as soon as the stress is released. The sensors showed a force sensitivity of 0.2542 $pF.mN^{-1}$ in a range from 3.5 mN to 17.5 mN, having a signal-to-noise ratio per unit force of 10.86.

Table 1: Comparative study of some of the significant research work in terms of the listed parameters.

Sl. No.	Fabrication technique	Materials processed	Limit of detection	Range	Sensitivity	Measurand	Reference
1.	Spin-coating	MWCNTs/PDMS	6 kPa	6-101 kPa	474.13 kPa^{-1}	Mechanical vibration and air pressure	[51]
2.	Self-assembly/ Casting	Polystyrene/PDMS	0	0–100 kPa	196 kPa^{-1}	Physiological movements, speech signals	[52]
3.	Self-assembly	Polystyrene/PDMS	0.1 kPa	0.1 -5 kPa	15 kPa^{-1}	Physiological signals	[53]
4.	In-situ polymerization	*N*, *N*′-methylene bis(acrylamide) (NNMBA)/ Ammonium persulphate (APS)	0.005 kPa	0.005 - 5 kPa	0.45 kPa^{-1} (> 30 Pa), 6.21 kPa^{-1} (4-25 Pa)	Tactile sensing	[54]
5.	DVD laser-scribing	Reduced graphene-oxide	0	0 - 50 kPa	0.96 kPa^{-1}	Tactile and pressure sensing	[55]
6.	Hummer's method/ Layer-by-layer assembly	Graphene/Gold nanoparticles/PDMS	86 Pa	86 – 53900 Pa	0.5 Pa^{-1}	Robotics, artificial skins	[56]
7.	Lithography/Spin-coating	Barium/titanate/Polyimide	0	0 -590 N	2.4 mV/N	In-situ force measurements	[8]
8.	Laser cutting/spin-coating	Copper/Tin/PDMS	0.5 N	0.5-27 N	0.34 ± 0.02 N^{-1}	Tactile sensing	[41]

The sensor patches were also attached to different daily-use objects to determine their capability to be used for real-time applications. The results show the potential for these sensor patches to be used as cheap and highly efficient force sensors, which can be used to develop low-cost, easy-to-fabricate systems for ubiquitous force-sensing monitoring applications. The capability of these sensors to measure such low forces increases their potential to be used in different touch-sensing applications, especially as soft-tactile sensors [57-59]. In comparison to the available research work done with 3D printed and Hall sensors, some of the advantages provided by these Graphite/PDMS sensors are higher dynamic range of force sensing, a capacitive method of sensing that provides a wide range of materials and low-resolution sensing and ability of communication at greater distances. Due to the biocompatible nature of the sensors, they can also be used in conjunction with implantable catheters for drug delivery and subsequent in-vivo changes. Other future work with these sensors would include their usage in real-time applications such as artificial skins (e-skins) to determine small touches on the body. They will be used as wearable sensors, embedded with signal-conditioning circuits for ubiquitous monitoring of the strain-induced applications. They can be incorporated with the clothes of a person to constantly monitor their physical health. Due to their ability to measure very low forces, they can also be employed for the detection of vital electrophysiological parameters like heartbeat, respiration, etc. These sensors can also be associated with prosthetic limbs to determine their capability for tactile sensing, replacing the currently used commercialized tactile sensors developed from materials like Dacron and Kevlar. They can also be used with robotics, where these sensors can provide information about the ambiance. From the fabrication point of view, the printed sensors can be associated with selective materials for biomolecular and biochemical sensing. The use of these sensors for other applications like temperature, gas, humidity, etc. sensing, can also be determined to validate their operation as multifunctional sensing systems.

Acknowledgement

The authors are obliged to the Microscopy Centre of Macquarie University, Australia for providing the SEM images of the developed sensor patches. They also thank Macquarie University for providing the research facilities to fabricate the sensor patches and perform experiments with them.

References

[1] P. Ruther, J. Bartholomeyczik, S. Trautmann, M. Wandt, O. Paul, W. Dominicus, et al., Novel 3D piezoresistive silicon force sensor for dimensional metrology of micro components, Sensors, 2005 IEEE, IEEE2005, p. 4 pp.
[2] D.J. Beebe, A.S. Hsieh, D.D. Denton, R.G. Radwin, A silicon force sensor for robotics and medicine, Sensors and Actuators A: Physical, 50(1995) 55-65.

[3] L. Beccai, S. Roccella, A. Arena, F. Valvo, P. Valdastri, A. Menciassi, et al., Design and fabrication of a hybrid silicon three-axial force sensor for biomechanical applications, Sensors and Actuators A: Physical, 120(2005) 370-82.
[4] P. Valdastri, S. Roccella, L. Beccai, E. Cattin, A. Menciassi, M. Carrozza, et al., Characterization of a novel hybrid silicon three-axial force sensor, Sensors and Actuators A: Physical, 123(2005) 249-57.
[5] Benefits of force sensors.
[6] W.S. Wong, A. Salleo, Flexible electronics: materials and applications: Springer Science & Business Media; 2009.
[7] R. Ouckama, D.J. Pearsall, Evaluation of a flexible force sensor for measurement of helmet foam impact performance, Journal of biomechanics, 44(2011) 904-9.
[8] K.-R. Lin, C.-H. Chang, T.-H. Liu, S.-W. Lin, C.-H. Lin, Experimental and numerical estimations into the force distribution on an occlusal surface utilizing a flexible force sensor array, Journal of biomechanics, 44(2011) 1879-84.
[9] S. El-Molla, A. Albrecht, E. Cagatay, P. Mittendorfer, G. Cheng, P. Lugli, et al., Integration of a thin film PDMS-based capacitive sensor for tactile sensing in an electronic skin, Journal of Sensors, 2016(2016).
[10] T.H. da Costa, J.-W. Choi, A flexible two dimensional force sensor using PDMS nanocomposite, Microelectronic Engineering, 174(2017) 64-9.
[11] J.A. Dobrzynska, M.A. Gijs, Flexible polyimide-based force sensor, Sensors and Actuators A: Physical, 173(2012) 127-35.
[12] M. Xie, K.C. Aw, W. Gao, Skin force sensor using piezoresistive PEDOT: PSS with arabitol on flexible PDMS, SENSORS, 2015 IEEE, IEEE2015, pp. 1-4.
[13] H. Kudo, T. Sawada, E. Kazawa, H. Yoshida, Y. Iwasaki, K. Mitsubayashi, A flexible and wearable glucose sensor based on functional polymers with Soft-MEMS techniques, Biosensors and Bioelectronics, 22(2006) 558-62.
[14] D.J. Cappelleri, G. Piazza, V. Kumar, Two-dimensional, vision-based μN force sensor for microrobotics, Robotics and Automation, 2009 ICRA'09 IEEE International Conference on, IEEE2009, pp. 1016-21.
[15] G.S. Heo, J. ho Choi, G.M. Kim, C.Y. Lee, PDMS membrane based force sensor: Basic structure design and assessment, Robotics (ISR), 2013 44th International Symposium on, IEEE2013, pp. 1-2.
[16] H. Jang, H. Yoon, Y. Ko, J. Choi, S.-S. Lee, I. Jeon, et al., Enhanced performance in capacitive force sensors using carbon nanotube/polydimethylsiloxane nanocomposites with high dielectric properties, Nanoscale, 8(2016) 5667-75.
[17] T.-L. Ren, H. Tian, D. Xie, Y. Yang, Flexible graphite-on-paper piezoresistive sensors, Sensors, 12(2012) 6685-94.
[18] X. Shuai, P. Zhu, W. Zeng, Y. Hu, X. Liang, Y. Zhang, et al., Highly Sensitive Flexible Pressure Sensor Based on Silver Nanowires-Embedded Polydimethylsiloxane Electrode with Microarray Structure, ACS applied materials & interfaces, 9(2017) 26314-24.
[19] Y. Kim, S. Park, S.K. Park, S. Yun, K.-U. Kyung, K. Sun, Transparent and flexible force sensor array based on optical waveguide, Optics express, 20(2012) 14486-93.
[20] H. Birol, T. Maeder, P. Ryser, Processing of graphite-based sacrificial layer for microfabrication of low temperature co-fired ceramics (LTCC), Sensors and Actuators A: Physical, 130(2006) 560-7.
[21] W.-P. Shih, L.-C. Tsao, C.-W. Lee, M.-Y. Cheng, C. Chang, Y.-J. Yang, et al., Flexible temperature sensor array based on a graphite-polydimethylsiloxane composite, Sensors, 10(2010) 3597-610.
[22] A.V. Kolliopoulos, J.P. Metters, C.E. Banks, Screen printed graphite electrochemical sensors for the voltammetric determination of antimony (III), Analytical Methods, 5(2013) 3490-6.
[23] R.R. Moore, C.E. Banks, R.G. Compton, Basal plane pyrolytic graphite modified electrodes: comparison of carbon nanotubes and graphite powder as electrocatalysts, Analytical chemistry, 76(2004) 2677-82.
[24] Z. Jing, Z. Guang-Yu, S. Dong-Xia, Review of graphene-based strain sensors, Chinese Physics B, 22(2013) 057701.
[25] J. Lu, I. Do, L.T. Drzal, R.M. Worden, I. Lee, Nanometal-decorated exfoliated graphite nanoplatelet based glucose biosensors with high sensitivity and fast response, ACS nano, 2(2008) 1825-32.
[26] S. Timur, L. Della Seta, N. Pazarlioğlu, R. Pilloton, A. Telefoncu, Screen printed graphite biosensors based on bacterial cells, Process Biochemistry, 39(2004) 1325-9.
[27] R.A. Antunes, M.C.L. De Oliveira, G. Ett, Investigation on the corrosion resistance of carbon black–graphite-poly (vinylidene fluoride) composite bipolar plates for polymer electrolyte membrane fuel cells, international journal of hydrogen energy, 36(2011) 12474-85.
[28] Y. Liu, Z. Ren, Y. Wei, B. Jiang, S. Feng, L. Zhang, et al., Synthesis and applications of graphite carbon sphere with uniformly distributed magnetic Fe 3 O 4 nanoparticles (MGCSs) and MGCS@ Ag, MGCS@ TiO 2, Journal of Materials Chemistry, 20(2010) 4802-8.
[29] H.J. Pandya, J. Sheng, J.P. Desai, MEMS-Based Flexible Force Sensor for Tri-Axial Catheter Contact Force Measurement, Journal of microelectromechanical systems, 26(2017) 264-72.
[30] D. Gräbner, M. Tintelott, G. Dumstorff, W. Lang, Low-Cost Thin and Flexible Screen-Printed Pressure Sensor, Multidisciplinary Digital Publishing Institute Proceedings2017, p. 616.
[31] A. Nag, S.C. Mukhopadhyay, J. Kosel, Tactile Sensing From Laser-Ablated Metallized PET Films, IEEE Sensors Journal, 17(2016) 7-13.
[32] M.O.F. Emon, J.-W. Choi, Flexible Piezoresistive Sensors Embedded in 3D Printed Tires, Sensors, 17(2017) 656.
[33] F. WASSERFALL, N. HENDRICH, F. FIEDLER, J. ZHANG, 3D-PRINTED LOW-COST MODULAR FORCE SENSORS.
[34] A. Kapoor, M. McKnight, K. Chatterjee, T. Agcayazi, H. Kausche, T. Ghosh, et al., Soft, flexible 3D printed fibers for capacitive tactile sensing, SENSORS, 2016 IEEE, IEEE2016, pp. 1-3.
[35] N. Wettels, V.J. Santos, R.S. Johansson, G.E. Loeb, Biomimetic tactile sensor array, Advanced Robotics, 22(2008) 829-49.
[36] T. Mei, W.J. Li, Y. Ge, Y. Chen, L. Ni, M.H. Chan, An integrated MEMS three-dimensional tactile sensor with large force range, Sensors and Actuators A: Physical, 80(2000) 155-62.
[37] M. Nie, H. Bao, Q.-A. Huang, J.G. Webster, Capacitive Pressure Sensors, Wiley Encyclopedia of Electrical and Electronics Engineering, John Wiley & Sons, Inc.1999.
[38] R.D.P. Wong, J.D. Posner, V.J. Santos, Flexible microfluidic normal force sensor skin for tactile feedback, Sensors and Actuators A: Physical, 179(2012) 62-9.
[39] M.I. Tiwana, A. Shashank, S.J. Redmond, N.H. Lovell, Characterization of a capacitive tactile shear sensor for application in robotic and upper limb prostheses, Sensors and Actuators A: Physical, 165(2011) 164-72.
[40] H.-K. Kim, S. Lee, K.-S. Yun, Capacitive tactile sensor array for touch screen application, Sensors and Actuators A: Physical, 165(2011) 2-7.
[41] L. Viry, A. Levi, M. Totaro, A. Mondini, V. Mattoli, B. Mazzolai, et al., Flexible three-axial force sensor for soft and highly sensitive artificial touch, Advanced Materials, 26(2014) 2659-64.
[42] H.-K. Lee, J. Chung, S.-I. Chang, E. Yoon, Real-time measurement of the three-axis contact force distribution using a flexible capacitive polymer tactile sensor, Journal of Micromechanics and Microengineering, 21(2011) 035010.
[43] Z. Wang, J. Wang, M. Li, K. Sun, C.-j. Liu, Three-dimensional printed acrylonitrile butadiene styrene framework coated with Cu-BTC metal-organic frameworks for the removal of methylene blue, Scientific reports, 4(2014).
[44] M.S.A. Rahman, S.C. Mukhopadhyay, P.-L. Yu, Novel Planar Interdigital Sensors, Novel Sensors for Food Inspection: Modelling, Fabrication and Experimentation, Springer2014, pp. 11-35.

[45] M. Schouten, R. Sanders, G. Krijnen, 3D printed flexible capacitive force sensor with a simple micro-controller based readout, SENSORS, 2017 IEEE, IEEE2017, pp. 1-3.
[46] A. Nag, S.C. Mukhopadhyay, J. Kosel, Flexible carbon nanotube nanocomposite sensor for multiple physiological parameter monitoring, Sensors and Actuators A: Physical, 251(2016) 148-55.
[47] A. Nag, N. Afasrimanesh, S. Feng, S.C. Mukhopadhyay, Strain induced graphite/PDMS sensors for biomedical applications, Sensors and Actuators A, 271(2018) 257-69.
[48] H. Yan, Y. Guo, S. Lai, X. Sun, Z. Niu, P. Wan, Flexible Room-Temperature Gas Sensors of Nanocomposite Network-Coated Papers, ChemistrySelect, 1(2016) 2816-20.
[49] A.V. Alaferdov, R. Savu, T. Rackauskas, S. Rackauskas, M. Canesqui, D. De Lara, et al., A wearable, highly stable, strain and bending sensor based on high aspect ratio graphite nanobelts, Nanotechnology, 27(2016) 375501.
[50] C. Min, D. Yu, J. Cao, G. Wang, L. Feng, A graphite nanoplatelet/epoxy composite with high dielectric constant and high thermal conductivity, Carbon, 55(2013) 116-25.
[51] Y. Meng, H. Li, K. Wu, S. Zhang, L. Li, High-Performance Pressure Sensor for Monitoring Mechanical Vibration and Air Pressure, Polymers, 10(2018) 587.
[52] Z. Wang, L. Zhang, J. Liu, H. Jiang, C. Li, Flexible hemispheric microarrays of highly pressure-sensitive sensors based on breath figure method, Nanoscale, 10(2018) 10691-8.
[53] Y. Zhang, Y. Hu, P. Zhu, F. Han, Y. Zhu, R. Sun, et al., Flexible and Highly Sensitive Pressure Sensor Based on Microdome-Patterned PDMS Forming with Assistance of Colloid Self-Assembly and Replica Technique for Wearable Electronics, ACS applied materials & interfaces, 9(2017) 35968-76.
[54] S. Zhang, F. Wang, H. Peng, J. Yan, G. Pan, Flexible highly sensitive pressure sensor based on ionic liquid gel film, ACS Omega, 3(2018) 3014-21.
[55] H. Tian, Y. Shu, X.-F. Wang, M.A. Mohammad, Z. Bie, Q.-Y. Xie, et al., A graphene-based resistive pressure sensor with record-high sensitivity in a wide pressure range, Scientific reports, 5(2015) 8603.
[56] M. Vaka, M.Z. Bian, N.D. Nam, Highly sensitive pressure sensor based on graphene hybrids, Arabian Journal of Chemistry, (2018).
[57] H. Wang, G. De Boer, J. Kow, M. Ghajari, A. Alazmani, R. Hewson, et al., A low-cost soft tactile sensing array using 3D Hall sensors, Procedia Engineering, Elsevier2016, pp. 650-3.
[58] H. Wang, G. de Boer, J. Kow, A. Alazmani, M. Ghajari, R. Hewson, et al., Design methodology for magnetic field-based soft tri-axis tactile sensors, Sensors, 16(2016) 1356.
[59] T. Paulino, P. Ribeiro, M. Neto, S. Cardoso, A. Schmitz, J. Santos-Victor, et al., Low-cost 3-axis soft tactile sensors for the human-friendly robot Vizzy, Robotics and Automation (ICRA), 2017 IEEE International Conference on, IEEE2017, pp. 966-71.